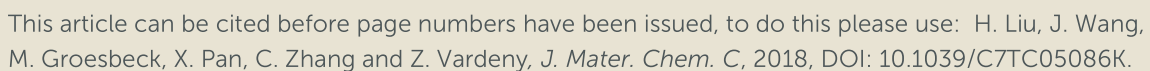


# Journal of Materials Chemistry C

Accepted Manuscript





This is an Accepted Manuscript, which has been through the Royal Society of Chemistry peer review process and has been accepted for publication.

Accepted Manuscripts are published online shortly after acceptance, before technical editing, formatting and proof reading. Using this free service, authors can make their results available to the community, in citable form, before we publish the edited article. We will replace this Accepted Manuscript with the edited and formatted Advance Article as soon as it is available.

You can find more information about Accepted Manuscripts in the <u>author guidelines</u>.

Please note that technical editing may introduce minor changes to the text and/or graphics, which may alter content. The journal's standard <u>Terms & Conditions</u> and the ethical guidelines, outlined in our <u>author and reviewer resource centre</u>, still apply. In no event shall the Royal Society of Chemistry be held responsible for any errors or omissions in this Accepted Manuscript or any consequences arising from the use of any information it contains.



We have investigated spin related processes in fullerene  $C_{60}$  devices using a several experimental techniques, which include magnetic field effect of photocurrent and electroluminescence in  $C_{60}$ -based diodes; spin polarized carrier injection in  $C_{60}$ -based spin-valves; and pure spin current generation in NiFe/ $C_{60}$ /Pt trilayer devices. We found that the 'curvature-related spin orbit coupling' in  $C_{60}$  plays a dominant role in the obtained spin-related phenomena. The measured magneto-photocurrent and magneto-electroluminescence responses in  $C_{60}$  diodes are dominated by the difference in the *g*-values of hole and electron polarons in the fullerene molecules. We also obtained giant magneto-resistance of ~10% at 10 K in  $C_{60}$  spin-valve devices, where spin polarized holes are injected into the  $C_{60}$  interlayer. In addition, using the technique of spin-pumping in NiFe/ $C_{60}$ /Pt trilayer devices with various  $C_{60}$  interlayer thicknesses we determined the spin diffusion length in  $C_{60}$  films to be  $13 \pm 2$  nm at room temperature.

<sup>\*</sup>To whom correspondence should be addressed: val@physics.utah.edu

# Introduction

Organic semiconductors (OSEC) have been widely studied over four decades since they show potential applications in optoelectronic devices such as organic light emitting diodes (OLED) [1], organic photovoltaic solar cells [2] and organic field-effect transistors [3]. Specifically, OLED have greatly advanced the display technology in industrial applications. In addition, OSEC have also become popular in the field of spintronics [4] due to their inherent long spin relaxation time compared with that in inorganic semiconductors. The small spin relaxation rates originate from the weak spin orbit coupling (SOC) and hyperfine interaction (HFI) in OSEC, because of the light atoms in their building blocks such as carbon and hydrogen, where the  $\pi$ -electrons play a dominant role in determining the electrical- and spin-related properties of the charge and neutral excitations.

Magneto-resistance in organic diodes, so called organic magneto-resistance (or OMAR), has been observed in various OSEC-based devices [5-8]. OMAR has been traditionally explained by invoking the SOC, which is an interaction that originates from nuclear charge and electron spin via their orbital motion, and hyperfine interaction (HFI) that is a more direct interaction between the nuclear and electron spins [9, 10]. These interactions dominate the inter-conversion between singlet and triplet polaron pair excitations, which is modulated when an external magnetic field is applied to the fdevice [11, 12]. This has been manifested in magneto-conductivity, magneto-photoconductivity and magneto-electroluminescence responses in various organic optoelectronic devices [13].

In addition to the magnetic field effect in organic diodes, where the electrodes are non-magnetic, giant magneto-resistance (GMR) has been also obtained in La<sub>2/3</sub>Sr<sub>1/3</sub>MnO<sub>3</sub> (LSMO)/OSEC/Co spin-valve devices [4, 14, 15], where the electrodes are ferromagnets (FM). The GMR response originates from a field induced change in the spin scattering rate between the two FM electrodes causing small (large) device resistance when the magnetizations of the two FM electrodes have parallel (antiparallel) configuration. In such devices the OSEC interlayer has been used for spin polarized carriers transport between the two FM electrodes, because of their relatively small spin-lattice relaxation rate. However the spin injection process is limited by the conductivity mismatch problem between the FM electrodes and the OSEC interlayer, and thus the ability to inject spin aligned carriers into the OSEC interlayer is crucially dependent on the FM/OSEC

spinterface states [16-18]. In contrast, pure spin current without the need of charge carrier injection has been recently shown to occur at FM/OSEC interface via the process of spin-pumping [19, 20]. In this case magnon excitations that are generated via FM-resonance (FMR), which carry spin-related angular momentum are scattered at the FM/OSEC interface resulting in excess angular momentum delivered to the electrons in the OSEC layer; this is called 'spin pumping' that leads to pure spin current in the OSEC film. The spin current in the OSEC layer may be detected by a Pt overlayer (which has large SOC) deposited onto the OSEC film, using the inverse spin Hall effect (ISHE) that converts spin-current into electrical current [21, 22]. This method may be used to effectively determine the spin diffusion length of the OSEC, if the measurements are repeated in trilayer FM/OSEC/Pt devices with various OSEC thicknesses.

On the occasion of Fred Wudl 50th anniversary of contribution to the field of Organic Optoelectronics we summarize here our recent investigations of spin-related properties in  $C_{60}$  devices. *Fullerenes, and especially*  $C_{60}$  have been one of the molecules that Fred loved to play with. Fullerene  $C_{60}$  is particularly suitable for spintronic applications since it contains ~99% naturally abundant  $^{12}$ C isotope having spinless nuclei, and thus negligible HFI constant. The intrinsic SOC in the  $C_{60}$  molecule is ~10 mK [23], so  $C_{60}$  is expected to have large spin diffusion length. However some experiments do not agree with this prediction[24, 25]. It has been theoretically found that the SOC strength,  $\xi$  is composed of intrinsic, curvature-related and Rashba terms [24, 26, 27]:  $\xi = \xi_{in} + \xi_{curv} + \xi_{Rashba}$ . Here  $\xi_{Rashba}$  is related to the inversion symmetry breaking and is negligible for  $C_{60}$ . Therefore the SOC strength in  $C_{60}$  is dominated by  $\xi_{curv}$  [24]. The spin polarized carrier transport in  $C_{60}$  has been even realized at room temperature by choosing suitable FM electrodes [25, 28]. In addition, spin photovoltaic and magnetic tunnel transistor devices based on  $C_{60}$  have been recently achieved [29, 30].

In this contribution, spin related effects have been investigated in various  $C_{60}$  based devices. We observed substantial magnetic field effect in  $C_{60}$  based diodes in spite of the negligible HFI strength in the fullerenes. We also obtained 10% GMR in LSMO/ $C_{60}$ /Co spin valves at 10 K, indicating efficient spin aligned carrier injection at the FM/ $C_{60}$  interface. In addition, we also determined the spin diffusion length in  $C_{60}$  films to be 13  $\pm$  2 nm from ISHE measurements in NiFe/ $C_{60}$ /Pt trilayer devices having various  $C_{60}$  thicknesses.

# **Experimental**

- (i)  $\underline{C}_{60}$  diodes: The  $C_{60}$  molecular structure is shown in Figure 1(a) inset. To form high quality thin films, the  $C_{60}$  powder (American Dye Source) was thermally evaporated in high vacuum chamber (1×10<sup>-7</sup> mbar) at a slow evaporation rate of ~0.05 nm/sec. The  $C_{60}$  diode was fabricated with the geometry of indium tin oxide (ITO) semitransparent anode, ~40 nm spin-cast polyethylenedioxythiophene/ polystyrene sulphonate (PEDOT:PSS) hole transport layer, ~200 nm  $C_{60}$  interlayer, that was capped with ~100 nm aluminum layer that serves as cathode. The device structure was thus ITO/PEDOT:PSS/ $C_{60}$ /Al with an active area of 2 × 2 mm<sup>2</sup>.
- (ii) <u>C<sub>60</sub>-based spin-valves</u>: The C<sub>60</sub> based spin-valve (SV) was fabricated using 15 nm C<sub>60</sub> thin film as spacer in between two FM electrodes, namely 20 nm patterned LSMO (bottom electrode, FM1) and 18 nm Co (top electrode, FM2), as shown in Figure 2(a). The device active crossed section area was  $200 \times 200 \,\mu\text{m}^2$ . The devices were placed in a cryostat with variable temperature control in between the two poles of an electromagnet with magnetic field up to 250 mT (having ~0.01 mT resolution). The FM/C<sub>60</sub> interface was characterized by tunneling electron microscopy (TEM) using a JEOL 2800 apparatus, and cross section view scanning electron microscopy (SEM) using a FEI Helios NanoLab 650 set-up. The magnetic hysteresis loops were measured by a home-made Sagnac MOKE with 10 nrad angular resolution [31].
- (iii) <u>C<sub>60</sub> devices for ISHE measurements</u>: The ISHE device was fabricated with 15 nm Ni<sub>80</sub>Fe<sub>20</sub> (NiFe) film on glass substrate, followed by C<sub>60</sub> layer with various thickness, and capped with 7 nm Pt connected with Cu wires to an electrometer for measuring the ISHE current induced by FMR in the NiFe film. The devices are covered with 100 nm SiO<sub>2</sub> protective layer. NiFe, Pt and SiO<sub>2</sub> were deposited by electron beam evaporation at a base pressure of 1×10<sup>-7</sup> mbar. The microstructure was characterized by cross section view SEM. The microwave (MW) for the ISHE measurements were generated by an Agilent N5173B amplifier working in the frequency range of 9 kHz to 20 GHz. The samples were put on top of MW guide of 250 μm wide transmission line with the radio frequency magnetic field perpendicular to the DC magnetic field. The ISHE voltage generated in the Pt overlayer was detected by phase-sensitive technique in which MW intensity was modulated by a square wave at 17 kHz.

# Results and discussion

# (i) Magnetic field effect in $C_{60}$ diodes

We studied the magnetic field effects (MFEs) in the  $C_{60}$  based diode device, which is given by the percentage change of a physical quantity upon the application of a field, B. For example, the magnetoconductivity response,  $MC(B) = 100\% \times (I(B)-I(0))/I(0)$ , where I denotes the electric current through the device. Figure 1(a) shows the current-voltage (I-V) and electroluminescence-voltage (EL-V) responses of an ITO/PEDOT: PSS/ $C_{60}$ /Al diode at room temperature, which are characteristic responses for organic diodes [24]. Figure 1(b) shows the change of current under applied in-plane magnetic field, MC(B) up to B=200 mT measured at a constant voltage of 18 V. MC(B) shows a negative response of nearly 2% having HWHM (half width at half maximum),  $B_0 \approx 17$  mT, which is much larger than  $B_0$  of MC(B) response based on HFI mechanism in conjugated polymers (of the order of 5 mT) [5]. We therefore infer that the underlying mechanism for the MC response here is not HFI, but the SOC in the  $C_{60}$  film. Since the internal SOC of carbon is small, we attribute the SOC in the  $C_{60}$  films as due to the curvature of the  $C_{60}$  molecule. The  $\pi$ -electrons do not possess any SOC; however the molecular curvature induces hybridization between the  $\pi$  and  $\sigma$  electrons, which leads to enhanced SOC in  $C_{60}$ .

As shown in Figure 1(c), the same  $C_{60}$  device was illuminated with a 405 nm diode laser, and the photocurrent at zero bias was measured as a function of the applied B field to obtain the magneto-photocurrent, MPC(B) response. We observed that the MPC(B) response increases and its HWHM decreases with increasing laser power, which could be explained by the defect generation within the  $C_{60}$  film upon irradiation[32]. We also observed electroluminescence (EL) from the same  $C_{60}$  device when it was operated at a high positive bias voltage. We therefore measure the EL intensity as a function of B field to obtain the magneto-EL response, MEL(B), as shown in Figure 1(d). It is worth mentioning that the MEL response has reversed polarity compared to that of MPC. This shows that the same process that increases the density of singlet excitons with B and thus leads to increase EL intensity and positive MEL; at the same time it decreases the density of photogenerated carriers that leads to a decrease in photocurrent and negative MPC.

In general, the HFI plays an important role in magnetic field effect in OSEC devices; however this is not the case for  $C_{60}$  since it has negligible nuclei spin. Moreover, all MFE(B) responses in the  $C_{60}$  devices are too broad to be explained based on the HFI mechanism (in which the MFE(B) width is typically  $\sim 5$  mT). We thus attribute the MFE here to the difference,  $\Delta g$  between the gfactors of the hole- and electron-polarons for the  $C_{60}$  molecules, the so called " $\Delta g$  mechanism" [33, 34]. In this process the spin of the hole- and electron-polarons in the induced spin ½ polaron-pair precesses around the field B at different rates, which results in a spin-mixing between singlet and triplet polaron pairs. We recall that the electron and hole g-factors in  $C_{60}$ , obtained using light induced electron spin resonance and doping measurements, respectively, are  $g_e = 1.9992$  for the electron-polaron and  $g_h = 2.0021$  for the hole-polaron [33, 35, 36]. Thus, under these conditions  $\Delta g$  is determined to be  $3x10^{-3}$  for the C<sub>60</sub> film. The HWHM,  $B_0$  of the MFE(B) response in the " $\Delta g$  model" is given by [28]:

$$B_0 = \frac{\hbar}{2\mu_B \Delta g \tau} \tag{1}$$

where  $\tau$  is the polaron spin coherence time, and  $\mu_B$  is the Bohr magneton. Using  $B_0 = 17$  mT and  $\Delta g = 3 \times 10^{-3}$  in Eq.(1) we estimate  $\tau \sim 110$  ns. This is in good agreement with other measurements of  $\tau$  in C<sub>60</sub> films using various coherent ODMR measuring techniques [37, 38].

### (ii) GMR in $C_{60}$ spin valves

Published on 14 February 2018. Downloaded by University of Windsor on 15/02/2018 14:31:39.

Spin polarized carriers' injection into and transport through  $C_{60}$  interlayer is realized in  $C_{60}$  based SV, as shown in Fig. 2. Figure 2(a) shows schematics and microstructure of the SV device. We note that the C<sub>60</sub>/Co interface is flat and very sharp. We may exclude leakage known to exist in organic SV devices based on the following TEM image. Figure 2(b) shows a high resolution TEM image of  $C_{60}$ /Co interface. It is clearly seen that the inter diffusion of Co clusters into the  $C_{60}$  film is  $\sim 2$  nm, if at all, and that the Co film is polycrystalline. The cross section view SEM image of the organic SV structure is also shown in Fig. S1. The energy dispersive spectroscopy of TEM (see Fig. S2) confirms that there are no inter diffusion clusters from the two FM electrodes. Figure 2(c) shows a typical GMR(B) response of the device for a bias voltage of 100 mV at 10 K. 15 nm  $C_{60}$  is sandwiched between two FM, namely LSMO with coercive field,  $B_1$ = 5 mT and Co having coercive field  $B_2 = 50$  mT at 10 K. Since the two FM have different coercive

fields, it is possible to switch the relative magnetization configuration of the FM electrodes between parallel and antiparallel upon sweeping the magnetic field, as seen in Fig. 2(b) insets. The corresponding magnetic hysteresis loop of the two FM electrodes in the device was characterized by MOKE using our extremely sensitive Sagnac interferometer[31], as seen in Fig. 2(d). Here GMR(B) response is defined as GMR(B)=[R(B)-R(P)]/R(P), where R(P) is the device resistance with parallel magnetization configuration of the two FM electrode. The maximum GMR value, GMR<sub>max</sub> may be described by the Julliere model:

$$\frac{\Delta R}{R} max = \frac{2P_1 P_2 e^{-d/\lambda_S}}{1 + P_1 P_2 e^{-d/\lambda_S}} \tag{2}$$

[39], where  $P_1$  and  $P_2$  are the spin polarization of the FM electrodes, and  $\lambda_s$  is the spin diffusion length in the C<sub>60</sub> film. We mention in passing that GMR<sub>max</sub> is strongly dependent on the spin injection properties at the FM/ $C_{60}$  interface, which is sensitive to the device fabrication processes. Figure 2(c) shows the bias voltage dependence of GMR<sub>max</sub> at 10 K. GMR<sub>max</sub> decreases with increasing the applied voltage. This may be related to the Fermi energy shift with the bias voltage, and consequent change of the effective spin polarizations of the LSMO and Co electrodes. The observed asymmetry of GMR<sub>max</sub> with V is widely reported in the literature [4, 40]. Figure 2(d) shows the temperature dependence of GMR<sub>max</sub>, which decreases with increasing temperature, T and vanishes at T≈250 K. The GMR<sub>max</sub> decrease with T is mainly due to the temperature dependence of the LSMO spin polarization, since its Curie phase transition temperature is below 300 K. We recall that the interaction between the organic molecules and FM atoms at the molecule/FM interface leads to the formation of chemical bonds [41-44], known as spinterface[16]. Such molecules may modify the magnetic properties of the FM electrodes [41, 45]. In addition the C<sub>60</sub> molecules may also be spin-polarized by the proximity effect of FM electrodes [43, 46].

### Spin pumping into $C_{60}$ films (iii)

Figure 3 describes the detection of pure spin current in C<sub>60</sub> film generated by the process of spin pumping. Figure 3(a) shows the schematics of the spin pumping process, spin transport through the C<sub>60</sub> interlayer, and spin detection in the Pt overlayer in the NiFe/C<sub>60</sub>/Pt trilayer device. The C<sub>60</sub>/Pt interface in the trilayer structure is characterized by cross section view SEM (see Fig. 3(a)), which shows a very clear and sharp interface. The spin current in C<sub>60</sub> is induced at the NiFe/C<sub>60</sub> interface by excess magnons due to the ferromagnetic resonance of the NiFe. The spin current in the C<sub>60</sub> film diffuses towards the other interface and reaches the C<sub>60</sub>/Pt interface while substantially attenuated. The C<sub>60</sub> spin current, in turn induces a spin current into the Pt overlayer, which is converted into electric current by the ISHE[19]. The C<sub>60</sub> spin current that arrives at the  $C_{60}/Pt$  interface is proportional to  $e^{-d/\lambda_s}$ , where d is the  $C_{60}$  film thickness. We note that by using this pure spin current pumping method, we can avoid the resistance mismatch and spinterface problems in SV devices. The upper panel of Fig. 3(b) shows the derivative of the MW absorption in the NiFe substrate under ferromagnetic resonance at room temperature. Consequently, an ISHE voltage is obtained in the Pt overlayer at the corresponding magnetic field, as shown in the lower panel of Fig. 3(b). Figure 3(c) shows the ISHE signal obtained in various NiFe/C<sub>60</sub>/Pt of different C<sub>60</sub> interlayer thicknesses. The sign changes of the ISHE voltage upon changing the magnetic field direction is a proof that we deal with ISHE and not due to several known artifacts, which is consistent with the ISHE theory [47]. Figure 3(d) shows the ISHE signal decay with increasing C<sub>60</sub> thickness, which can be well fitted by the relation  $V_{ISHE} \propto e^{-d/\lambda_s}$ . From the fit to the obtained data we estimate the spin diffusion length of  $C_{60}$  at room temperature to be  $\lambda_s = 13 \pm$ 2 nm.

# **Conclusions**

In summary, we have studied the spin-mixing mechanism of spin ½ polaron pairs, spin polarized carrier transport and pure spin current transport in a series of C<sub>60</sub> thin-film devices. Although the HFI in C<sub>60</sub> films is miniature, SOC still exists due to the 'curvature induced hybridization' between the  $\pi$  and  $\sigma$  electrons of the spherical molecule, and is strong enough to influence the spin-related effects in C<sub>60</sub> films. The magnetic field responses in C<sub>60</sub> diodes with non-magnetic electrodes such as MPC, MC and MEL are interpreted as due to the "Δg mechanism" between the electron and hole in the  $C_{60}$  film. From the HWHM of the MFE(B) responses we obtained the spin lifetime of polaron pair  $\sim$ 110 ns. In addition we obtained GMR of  $\sim$ 10% in C<sub>60</sub> based SV devices at low temperature. The bias voltage and temperature dependences of the measured GMR are similar to that in other organic SVs. The generation of pure spin current in C<sub>60</sub> films has been realized based on the spin pumping effect; from its C<sub>60</sub> interlayer thickness dependence we obtained the spin diffusion length in  $C_{60}$  films to be  $\lambda_s = 13 \pm 2$  nm at room temperature.

These findings imply the great potentials of fullerene-based materials in studying spin-related phenomena and fabricating novel effective organic spintronic devices.

## Acknowledgements

This work was supported by the NSF grant DMR-1701427. The device fabrication facility has been supported by the NSF-MRSEC program DMR 1121252 at the University of Utah.

# References

- [1] J.H. Burroughes, D.D.C. Bradley, A.R. Brown, R.N. Marks, K. Mackay, R.H. Friend, P.L. Burns, A.B. Holmes, Light-emitting diodes based on conjugated polymers, Nature, 347 (1990) 539-541.
- [2] A.J. Heeger, 25th Anniversary Article: Bulk Heterojunction Solar Cells: Understanding the Mechanism of Operation, Advanced Materials, 26 (2014) 10-28.
- [3] C.D. Dimitrakopoulos, P.R.L. Malenfant, Organic Thin Film Transistors for Large Area Electronics, Advanced Materials, 14 (2002) 99-117.
- [4] Z.H. Xiong, D. Wu, Z. Valy Vardeny, J. Shi, Giant magnetoresistance in organic spin-valves, Nature, 427 (2004) 821-824.
- [5] T.D. Nguyen, Y. Sheng, J. Rybicki, G. Veeraraghavan, M. Wohlgenannt, Magnetoresistance in [small pi]-conjugated organic sandwich devices with varying hyperfine and spin-orbit coupling strengths, and varying dopant concentrations, Journal of Materials Chemistry, 17 (2007) 1995-2001.
- [6] V.N. Prigodin, J.D. Bergeson, D.M. Lincoln, A.J. Epstein, Anomalous room temperature magnetoresistance in organic semiconductors, Synthetic Metals, 156 (2006) 757-761.
- [7] P.A. Bobbert, T.D. Nguyen, F.W.A. van Oost, B. Koopmans, M. Wohlgenannt, Bipolaron Mechanism for Organic Magnetoresistance, Physical Review Letters, 99 (2007) 216801.
- [8] B. Hu, Y. Wu, Tuning magnetoresistance between positive and negative values in organic semiconductors, 6 (2007) 985.
- [9] R. Geng, N.T. Mayhew, T.D. Nguyen, Tunable magneto-conductance and magneto-electroluminescence in polymer light-emitting electrochemical planar devices, Applied Physics Letters, 103 (2013) 243307.
- [10] Y. Sheng, T.D. Nguyen, G. Veeraraghavan, Ö. Mermer, M. Wohlgenannt, S. Qiu, U. Scherf, Hyperfine interaction and magnetoresistance in organic semiconductors, Physical Review B, 74 (2006) 045213.
- [11] L. Nuccio, M. Willis, L. Schulz, S. Fratini, F. Messina, M. D'Amico, F.L. Pratt, J.S. Lord, I. McKenzie, M. Loth, B. Purushothaman, J. Anthony, M. Heeney, R.M. Wilson, I. Hernández, M. Cannas, K. Sedlak, T. Kreouzis, W.P. Gillin, C. Bernhard, A.J. Drew, Importance of Spin-Orbit Interaction for the Electron Spin Relaxation in Organic Semiconductors, Physical Review Letters, 110 (2013) 216602.
- [12] P. Shakya, P. Desai, M. Somerton, G. Gannaway, T. Kreouzis, W.P. Gillin, The magnetic field effect on the transport and efficiency of group III tris(8-hydroxyquinoline) organic light emitting diodes, Journal of Applied Physics, 103 (2008) 103715.
- [13] R. Geng, T.T. Daugherty, K. Do, H.M. Luong, T.D. Nguyen, A review on organic spintronic materials and devices: I. Magnetic field effect on organic light emitting diodes, Journal of Science: Advanced Materials and Devices, 1 (2016) 128-140.

- [14] A.J. Drew, J. Hoppler, L. Schulz, F.L. Pratt, P. Desai, P. Shakya, T. Kreouzis, W.P. Gillin, A. Suter, N.A. Morley, V.K. Malik, A. Dubroka, K.W. Kim, H. Bouyanfif, F. Bourqui, C. Bernhard, R. Scheuermann, G.J. Nieuwenhuys, T. Prokscha, E. Morenzoni, Direct measurement of the electronic spin diffusion length in a fully functional organic spin valve by low-energy muon spin rotation, 8 (2008) 109.
- [15] M. Cinchetti, K. Heimer, J.-P. Wüstenberg, O. Andreyev, M. Bauer, S. Lach, C. Ziegler, Y. Gao, M. Aeschlimann, Determination of spin injection and transport in a ferromagnet/organic semiconductor heterojunction by two-photon photoemission, 8 (2008) 115.
- [16] C. Barraud, P. Seneor, R. Mattana, S. Fusil, K. Bouzehouane, C. Deranlot, P. Graziosi, L. Hueso, I. Bergenti, V. Dediu, F. Petroff, A. Fert, Unravelling the role of the interface for spin injection into organic semiconductors, Nat Phys, 6 (2010) 615-620.
- [17] F. Djeghloul, F. Ibrahim, M. Cantoni, M. Bowen, L. Joly, S. Boukari, P. Ohresser, F. Bertran, P. Le Fèvre, P. Thakur, F. Scheurer, T. Miyamachi, R. Mattana, P. Seneor, A. Jaafar, C. Rinaldi, S. Javaid, J. Arabski, J.P. Kappler, W. Wulfhekel, N.B. Brookes, R. Bertacco, A. Taleb-Ibrahimi, M. Alouani, E. Beaurepaire, W. Weber, Direct observation of a highly spin-polarized organic spinterface at room temperature, Scientific Reports, 3 (2013) 1272.
- [18] D.L. Smith, R.N. Silver, Electrical spin injection into semiconductors, Physical Review B, 64 (2001) 045323.
- [19] S. Watanabe, K. Ando, K. Kang, S. Mooser, Y. Vaynzof, H. Kurebayashi, E. Saitoh, H. Sirringhaus, Polaron spin current transport in organic semiconductors, Nat Phys, 10 (2014) 308-313.
- [20] D. Sun, K.J. van Schooten, M. Kavand, H. Malissa, C. Zhang, M. Groesbeck, C. Boehme, Z. Valy Vardeny, Inverse spin Hall effect from pulsed spin current in organic semiconductors with tunable spin-orbit coupling, Nat Mater, 15 (2016) 863-869.
- [21] E. Saitoh, M. Ueda, H. Miyajima, G. Tatara, Conversion of spin current into charge current at room temperature: Inverse spin-Hall effect, Applied Physics Letters, 88 (2006) 182509.
- [22] K. Ando, S. Watanabe, S. Mooser, E. Saitoh, H. Sirringhaus, Solution-processed organic spin—charge converter, Nat Mater, 12 (2013) 622-627.
- [23] D. Huertas-Hernando, F. Guinea, A. Brataas, Spin-orbit coupling in curved graphene, fullerenes, nanotubes, and nanotube caps, Physical Review B, 74 (2006) 155426.
- [24] S. Liang, R. Geng, B. Yang, W. Zhao, R. Chandra Subedi, X. Li, X. Han, T.D. Nguyen, Curvature-enhanced Spin-orbit Coupling and Spinterface Effect in Fullerene-based Spin Valves, 6 (2016) 19461.
- [25] M. Gobbi, F. Golmar, R. Llopis, F. Casanova, L.E. Hueso, Room-Temperature Spin Transport in C60-Based Spin Valves, Advanced Materials, 23 (2011) 1609-1613.
- [26] G.A. Steele, F. Pei, E.A. Laird, J.M. Jol, H.B. Meerwaldt, L.P. Kouwenhoven, Large spin-orbit coupling in carbon nanotubes, 4 (2013) 1573.
- [27] H. Min, J.E. Hill, N.A. Sinitsyn, B.R. Sahu, L. Kleinman, A.H. MacDonald, Intrinsic and Rashba spin-orbit interactions in graphene sheets, Physical Review B, 74 (2006) 165310.
- [28] X. Zhang, S. Mizukami, T. Kubota, Q. Ma, M. Oogane, H. Naganuma, Y. Ando, T. Miyazaki, Observation of a large spin-dependent transport length in organic spin valves at room temperature, Nature Communications, 4 (2013) 1392.
- [29] X. Sun, S. Vélez, A. Atxabal, A. Bedoya-Pinto, S. Parui, X. Zhu, R. Llopis, F. Casanova, L.E. Hueso, A molecular spin-photovoltaic device, Science, 357 (2017) 677-680.
- [30] M. Gobbi, A. Bedoya-Pinto, F. Golmar, R. Llopis, F. Casanova, L.E. Hueso, C60-based hot-electron magnetic tunnel transistor, Applied Physics Letters, 101 (2012) 102404.
- [31] R. McLaughlin, D. Sun, C. Zhang, M. Groesbeck, Z.V. Vardeny, Optical detection of transverse spin-Seebeck effect in permalloy film using Sagnac interferometer microscopy, Physical Review B, 95 (2017) 180401.
- [32] B.R. Gautam, T.D. Nguyen, E. Ehrenfreund, Z.V. Vardeny, Magnetic field effect on excited-state spectroscopies of \$\ensuremath{\pi}\$-conjugated polymer films, Physical Review B, 85 (2012) 205207.

- [34] C. Zhang, D. Sun, C.X. Sheng, Y.X. Zhai, K. Mielczarek, A. Zakhidov, Z.V. Vardeny, Magnetic field effects in hybrid perovskite devices, Nat Phys, 11 (2015) 427-434.
- [35] P.M. Allemand, G. Srdanov, A. Koch, K. Khemani, F. Wudl, Y. Rubin, F. Diederich, M.M. Alvarez, S.J. Anz, R.L. Whetten, The unusual electron spin resonance of fullerene C60 anion radical, Journal of the American Chemical Society, 113 (1991) 2780-2781.
- [36] L. Dunsch, F. Ziegs, C. Siedschlag, J. Mattay, ESR Spectroscopy of the C60 Cation Produced by Photoinduced Electron Transfer, Chemistry A European Journal, 6 (2000) 3547-3550.
- [37] W. Harneit, C. Boehme, S. Schaefer, K. Huebener, K. Fostiropoulos, K. Lips, Room Temperature Electrical Detection of Spin Coherence in \${\mathrm{C}}\_{60}\$, Physical Review Letters, 98 (2007) 216601.
- [38] M.N. Uvarov, L.V. Kulik, M.A. Bizin, V.N. Ivanova, R.B. Zaripov, S.A. Dzuba, Anisotropic Pseudorotation of the Photoexcited Triplet State of Fullerene C60 in Molecular Glasses Studied by Pulse EPR, The Journal of Physical Chemistry A, 112 (2008) 2519-2525.
- [39] M. Julliere, Tunneling between ferromagnetic films, Physics Letters A, 54 (1975) 225-226.
- [40] J. Devkota, R. Geng, R.C. Subedi, T.D. Nguyen, Organic Spin Valves: A Review, Advanced Functional Materials, 26 (2016) 3881-3898.
- [41] M. Sun, D. Zheng, X. Wang, W. Mi, Electric Field Tunable Magnetism at C6H6-Adsorbed Fe3O4(001) Surface, The Journal of Physical Chemistry C, 121 (2017) 5178-5184.
- [42] Q. Zhang, W. Mi, X. Wang, Antiferromagnetic Order at The First Fe4N Atomic Layer in Benzene Adsorbed Fe4N Structures, The Journal of Physical Chemistry C, 119 (2015) 23619-23626.
- [43] M. Sun, X. Wang, W. Mi, Spin polarization and magnetic characteristics at C6H6/Co2MnSi(001) spinterface, The Journal of Chemical Physics, 147 (2017) 114702.
- [44] Q. Zhang, L. Yin, W. Mi, X. Wang, Large Spatial Spin Polarization at Benzene/La2/3Sr1/3MnO3 Spinterface: Toward Organic Spintronic Devices, The Journal of Physical Chemistry C, 120 (2016) 6156-6164.
- [45] K. Bairagi, A. Bellec, V. Repain, C. Chacon, Y. Girard, Y. Garreau, J. Lagoute, S. Rousset, R. Breitwieser, Y.-C. Hu, Y.C. Chao, W.W. Pai, D. Li, A. Smogunov, C. Barreteau, Tuning the Magnetic Anisotropy at a Molecule-Metal Interface, Physical Review Letters, 114 (2015) 247203.
- [46] A. Droghetti, P. Thielen, I. Rungger, N. Haag, N. Großmann, J. Stöckl, B. Stadtmüller, M. Aeschlimann, S. Sanvito, M. Cinchetti, Dynamic spin filtering at the Co/Alq3 interface mediated by weakly coupled second layer molecules, Nature Communications, 7 (2016) 12668.
- [47] K. Ando, S. Takahashi, J. Ieda, Y. Kajiwara, H. Nakayama, T. Yoshino, K. Harii, Y. Fujikawa, M. Matsuo, S. Maekawa, E. Saitoh, Inverse spin-Hall effect induced by spin pumping in metallic system, Journal of Applied Physics, 109 (2011) 103913.

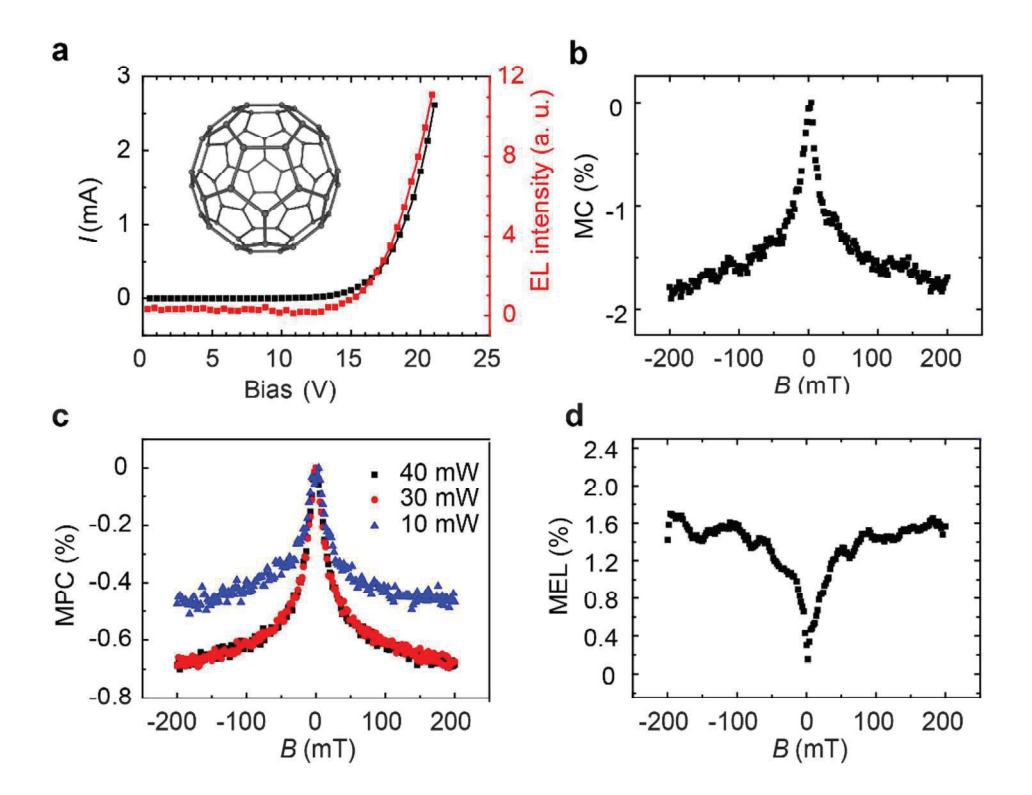


Figure 1. Magnetic field effects in the  $C_{60}$  based device. a, I-V (black) and EL-V (red) device responses at forward bias. Inset: molecular structure of  $C_{60}$ . b, MC(B) response measured at applied bias voltage of 18 V at room temperature. c, MPC(B) response under illumination of 405 nm laser at different laser powers, as given. d, MEL(B) response from the same device measured at positive bias voltage of 20 V.

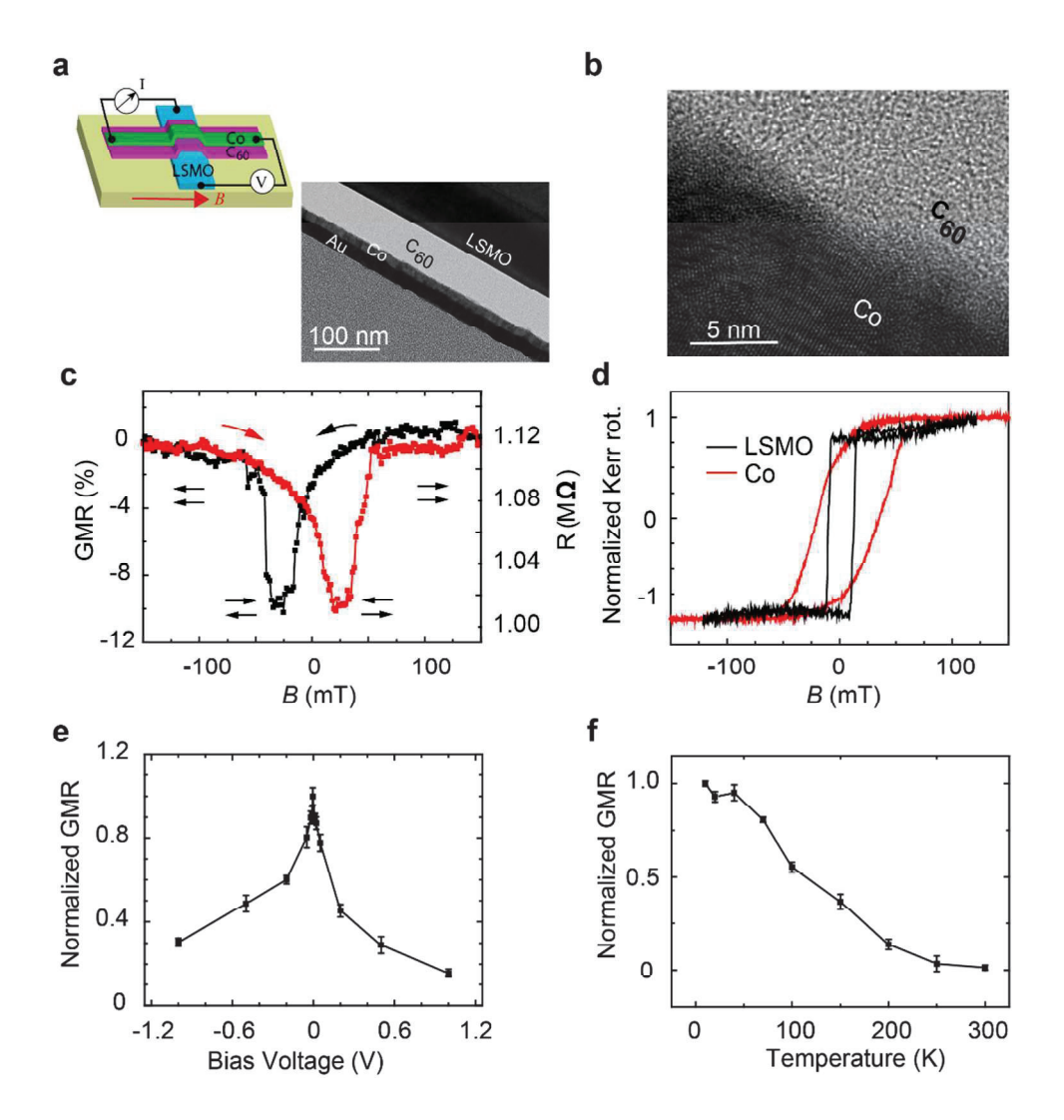


Figure 2. GMR in  $C_{60}$  based SV devices. a, Schematics of the SV device structure and a typical low resolution TEM image. Here the  $C_{60}$  film is sandwiched between two ferromagnet electrodes, namely LSMO and Co. The current change under a fixed voltage is recorded when sweeping the magnetic field. b, High resolution TEM image of the  $C_{60}$ /Co interface. c, GMR(B) response in LSMO (20 nm)/ $C_{60}$  (15 nm)/Co (30 nm) SV measured at an applied bias voltage of 100 mV. The maximum GMR, GMR<sub>max</sub> value is ~10%. d, the magnetic hysteresis loops of the spin valve device measured by MOKE using a Sagnac intergferometer. e and f, bias voltage and temperature dependencies of the measured GMR<sub>max</sub>.

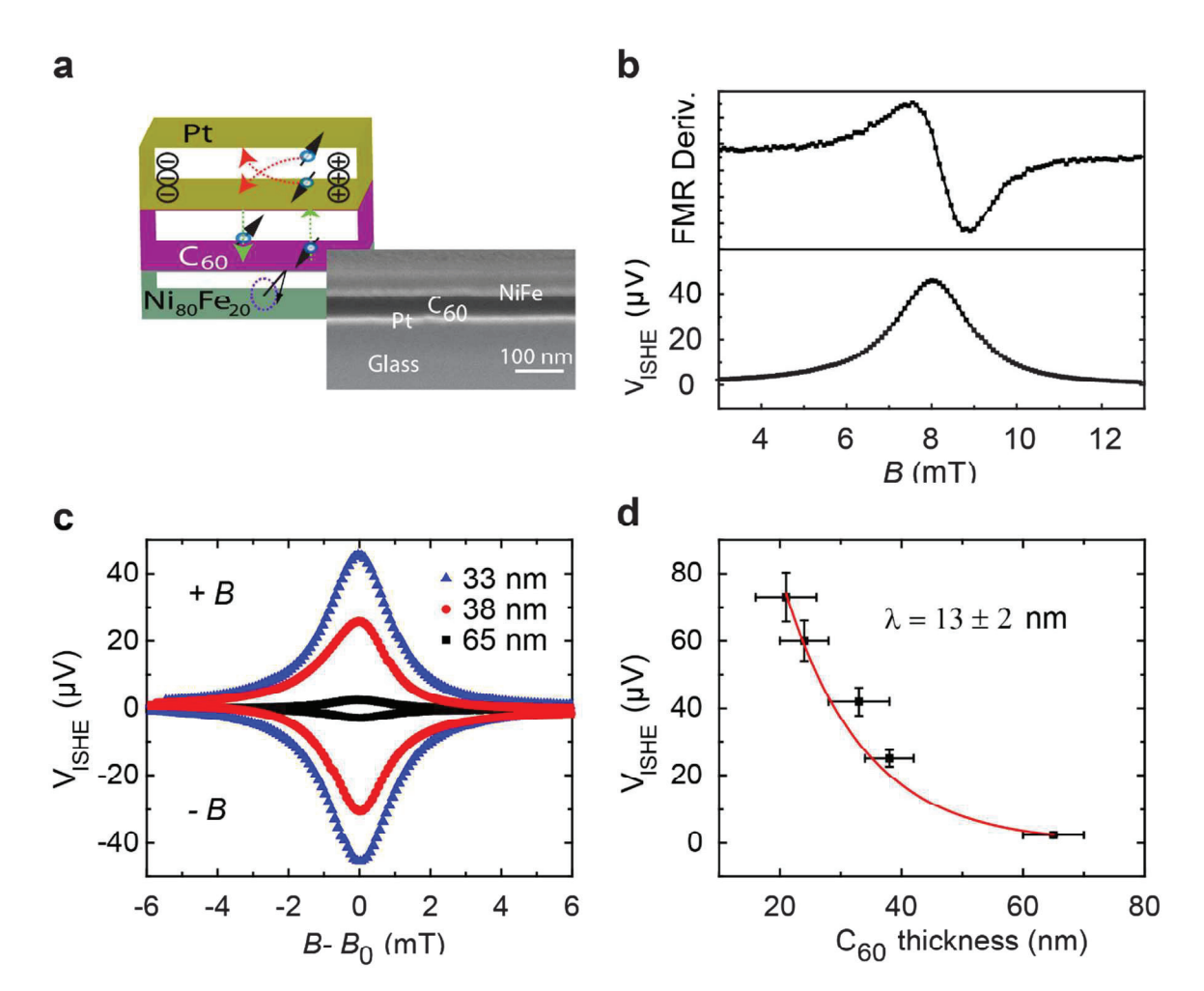


Figure 3. Pure spin current generation in and transport through  $C_{60}$  film based on the spin-pumping effect. a, schematics and microstructure of the device. The microstructure is characterized by cross section view of SEM. The NiFe FM substrate operates at magnetic resonance condition that generates excess magnon excitations. Spin angular momentum carried by the magnons is transferred to the  $C_{60}$  electrons at the NiFe/ $C_{60}$  interface via the spin-pumping effect. The induced spin current in the  $C_{60}$  film diffuses away from the NiFe/ $C_{60}$  interface and reaches the  $C_{60}$ /Pt interface. The induced spin current in the Pt overlayer is converted into electrical current via the ISHE. The magnetization, spin current and electric current directions are all perpendicular to each other. b, derivative of the microwave absorption in the NiFe film at FMR condition (upper panel) and corresponding ISHE signal obtained in the Pt overlayer (lower panel) at room temperature. c, ISHE signals obtained in Pt layer of NiFe/ $C_{60}$ /Pt trilayer devices having various  $C_{60}$  interlayer thicknesses. The sign change of the ISHE voltage is due to the reversal of the magnetic field direction.  $B_0$  is resonant field. d,  $C_{60}$  interlayer thickness

dependence of the ISHE voltage measured from the Pt overlayer. The red line is an exponential fit, from which we obtain the spin diffusion length in  $C_{60}$  as given.